

Hodge-Decomposition of Brain Networks

D Vijay Anand¹, Moo K. Chung² email: mkchung@wisc.edu

¹ University College London, UK ² University of Wisconsin-Madison, USA

Introduction

We decompose rs-fMRI brain networks into three orthogonal components—gradient, curl, and harmonic flows—through Hodge decomposition (Fig. 1) and quantify these components using the Wasserstein distance.

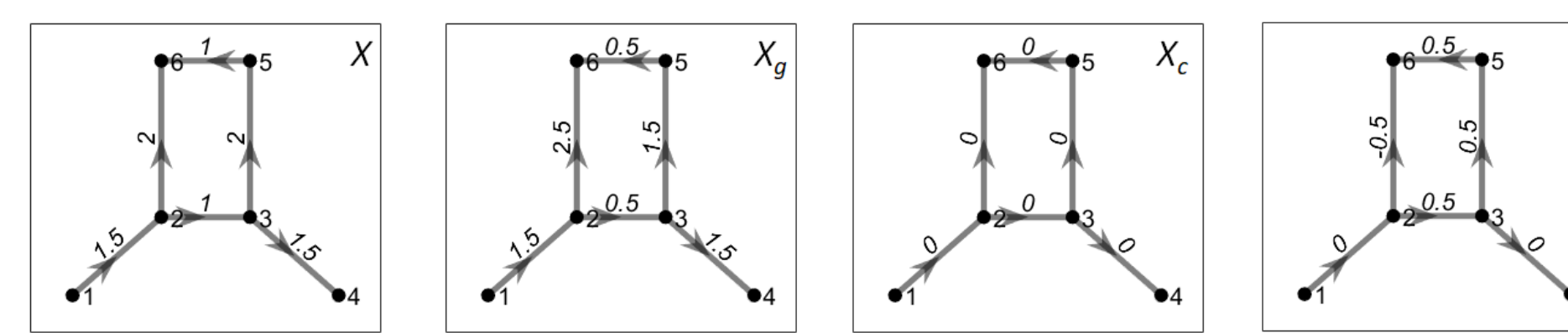


Fig. 1. Hodge decomposition on edge flow X is decomposed into gradient, curl and harmonic components.

Boundary and Coboundary Operators

A simplicial complex is a collection of simplices including nodes (0-simplices), edges (1-simplices), triangles (2-simplices), and their higher-dimensional counterparts. A k -chain is a linear combination of k -simplices, forming a group \mathcal{K}_k . The boundary operator $\partial_k : \mathcal{K}_k \rightarrow \mathcal{K}_{k-1}$ for a k -simplex σ_k is defined as

$$\partial_k(\sigma_k) = \sum_{i=0}^k (-1)^i(v_0, \dots, \hat{v_i}, \dots, v_k),$$

where $(v_0, \dots, \hat{v_i}, \dots, v_k)$ are the $(k-1)$ -faces of σ_k , obtained by omitting vertex $\hat{v_i}$. The corresponding boundary matrix \mathbb{B}_k generalizes the incidence matrix to higher dimensions (Anand and Chung, 2023). Coboundary operators δ_k are duals of the boundary operators, mapping k -cochains to $(k+1)$ -cochains: $\delta_k : \mathcal{K}^k \rightarrow \mathcal{K}^{k+1}$. The coboundary matrix is the transpose of the boundary matrix: $\delta_k = \mathbb{B}_{k+1}^\top$.

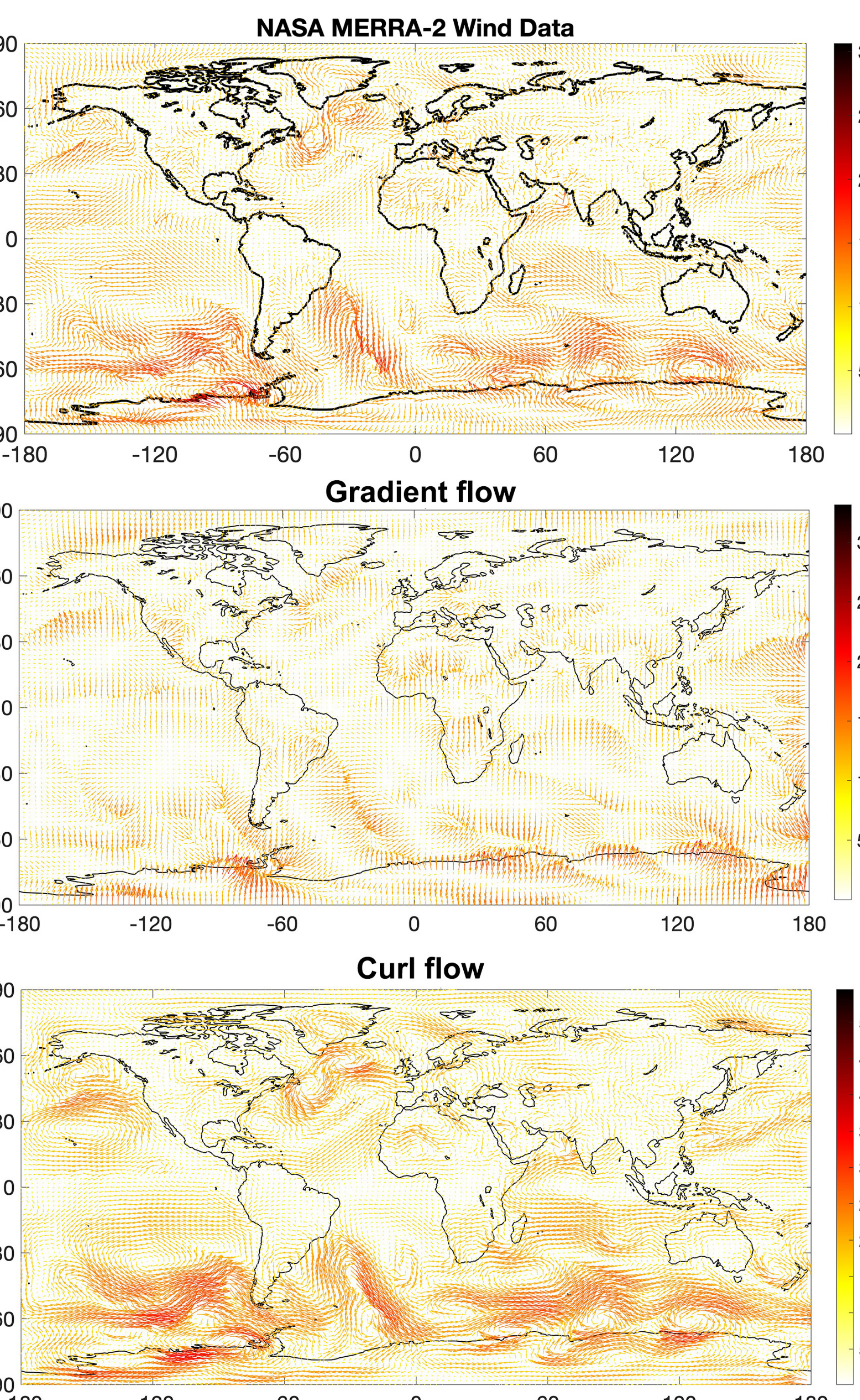


Fig. 2. Illustration of the Hodge decomposition, which breaks down the wind field into gradient and curl flows. This method can similarly decompose network edge flows into orthogonal components.

Hodge Decomposition

Let C^k be the space of functions over k -simplices. The Hodge decomposition separates an edge flow $X \in C^1$ into three orthogonal components: gradient X_G , curl X_C , and harmonic flows X_H :

$$X = X_G + X_C + X_H = \delta_0 s + \delta_1^\top \phi + X_H,$$

with potential functions $s \in C^1$ and $\phi \in C^2$ (Fig. 1 and 2). X_G and X_C are obtained by minimizing the projection residuals. The harmonic component $X_H = X - (X_G + X_C)$ is estimated as the residual. The sum of the curl and harmonic components forms the loop flow, while the gradient component is the non-loop flow.

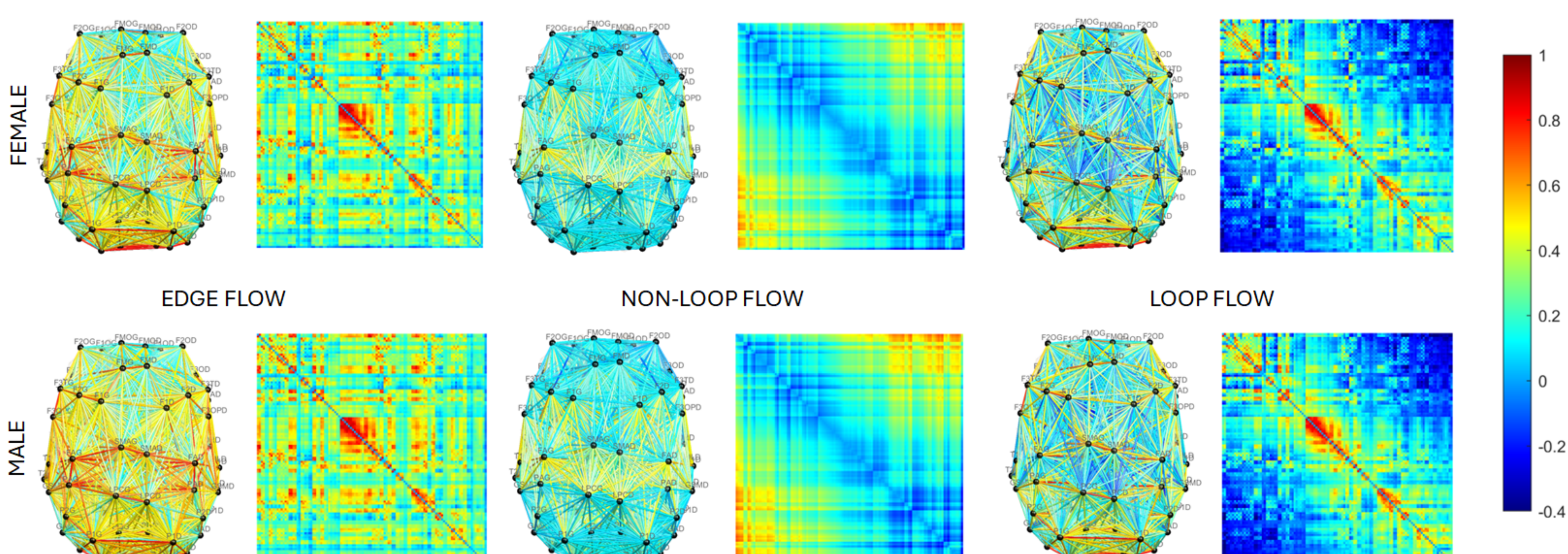


Fig. 3. The average connectivity (edge flow), non-loop flow (middle), which is gradient flow X_G , and the loop flow (right), which is the sum of curl X_C and harmonic flow X_H and corresponding connectivity matrices.

Topological Inference

Topological differences between two groups of networks, $\Omega = \{\Omega_1, \Omega_2, \dots, \Omega_m\}$ and $\Psi = \{\Psi_1, \Psi_2, \dots, \Psi_n\}$, are computed using the Wasserstein distance (Anand and Chung, 2023):

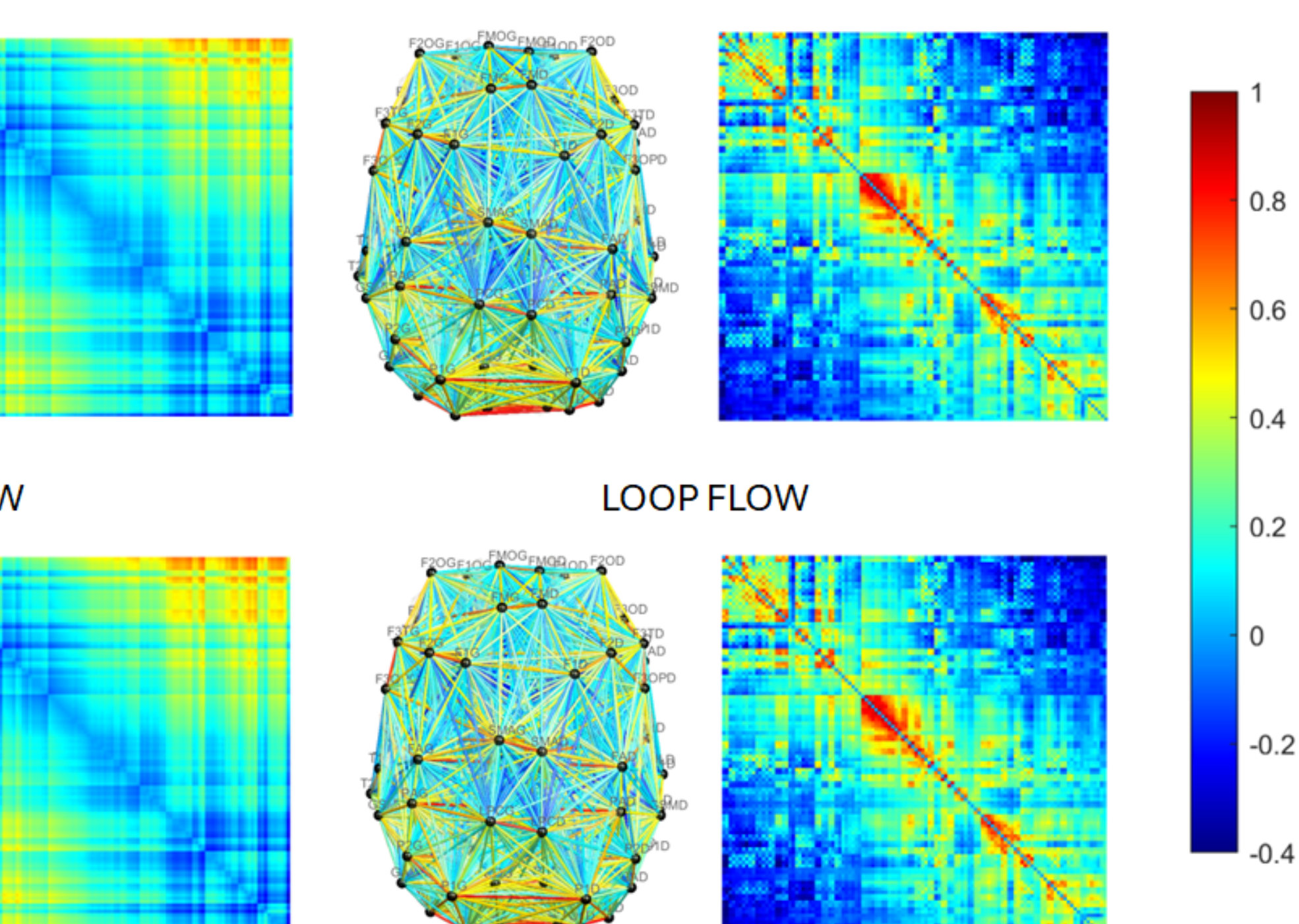
$$\mathfrak{L}_\infty^b = \max_{1 \leq j \leq q_0} |\bar{b}_j^\Omega - \bar{b}_j^\Psi|, \quad \mathfrak{L}_\infty^d = \max_{1 \leq j \leq q_1} |\bar{d}_j^\Omega - \bar{d}_j^\Psi|$$

where \bar{b}_j^Ω and \bar{b}_j^Ψ are the means of the j -th smallest birth values of connected components in Ω and Ψ , and \bar{d}_j^Ω and \bar{d}_j^Ψ are the means of the j -th smallest death values of cycles in Ω and Ψ (Das et al., 2023). Here, q_0 and q_1 are the number of birth and death values, respectively. The combined metric $\mathfrak{L}_\infty(\Omega, \Psi) = \mathfrak{L}_\infty^b + \mathfrak{L}_\infty^d$ is also used. The permutation test determines statistical significance. Simulation results based on random modular networks are given in Table 1.

Nodes	Modules	<i>p</i> -values		
		<i>p</i>	<i>c</i>	Edge Loop Non-loop
12 vs. 12	2 vs. 3	0.0001	0.0039	0.0000
	3 vs. 6	0.0011	0.0005	0.0002
18 vs. 18	2 vs. 3	0.0000	0.0012	0.0000
	3 vs. 6	0.0003	0.0001	0.0001
24 vs. 24	2 vs. 3	0.0000	0.0001	0.0000
	3 vs. 6	0.0000	0.0001	0.0000
24 vs. 24	2 vs. 2	0.1135	0.9669	0.1794
	3 vs. 3	0.5348	0.7451	0.8864
	6 vs. 6	0.2863	0.4055	0.6055

Table 1. The performance results of the Wasserstein distance \mathfrak{L}_∞ on the edge, loop and non-loop flows. Smaller *p*-values are better when there are network differences (top rows) and larger *p*-values are better when there are no network differences (bottom rows).

MATLAB code for the Hodge decomposition is available at <https://github.com/laqlcebeltrami/hodge>. The estimation is done through the least squares estimation using the boundary and coboundary matrices.



Application

We used resting-state fMRI (rs-fMRI) data from the Human Connectome Project comprising of 400 subjects (168 males, 232 females) (Huang et al., 2020). Fig. 3 shows the Hodge decomposition applied to average female and male brain networks. The topological differences between the groups was assessed using the Wasserstein distances \mathfrak{L}_∞^b and \mathfrak{L}_∞^d with permutation tests ($p = 0.0177, 0.0110$). We also tested the decomposed components: gradient ($p = 0.008$), and curl ($p = 0.0296$). For the non-loop component (gradient flow), permutation tests yielded *p*-values of 0.0088 (birth) and 0.0080 (death). For loop components (curl and harmonic combined), *p*-values were 0.0019 (birth) and 0.1582 (death).

Funding. NIH EB028753, MH133614 and NSF MDS-2010778.

References

- D.V. Anand and M.K. Chung. Hodge-Laplacian of brain networks. *IEEE Transactions on Medical Imaging*, 42:1563–1473, 2023.
- S. Das, D.V. Anand, and M.K. Chung. Topological data analysis of human brain networks through order statistics. *PLOS One*, 18(3): e0276419, 2023.
- S.-G. Huang, S.-T. Samdin, C.M. Ting, H. Ombao, and M.K. Chung. Statistical model for dynamically-changing correlation matrices with application to brain connectivity. *Journal of Neuroscience Methods*, 331:108480, 2020.